https://doi.org/10.5194/egusphere-2026-4083
Preprint. Discussion started: 21 July 2026

Automatic classification of the hydrothermal structure of polythermal glaciers from ground-penetrating radar using deep learning techniques

Unai Letamendia[1], Iván Ramírez[2], Francisco Navarro[1], Beatriz Benjumea[3], Ivan Lavrentiev[4], and Emanuele Schiavi[5]

[1]ETSI de Telecomunicación, Universidad Politécnica de Madrid, Madrid, Spain
[2]Computer Science and Statistics Department, Universidad Rey Juan Carlos, Madrid, Spain
[3]Instituto Geológico y Minero de España-CSIC, Madrid, Spain
[4]Institute of Geography, Russian Academy of Sciences, Moscow, Russia
[5]Department of Applied Mathematics, Universidad Rey Juan Carlos, Madrid, Spain

Correspondence: Unai Letamendia (unai.letamendia@upm.es)

Abstract. Knowing the internal spatial distribution of cold and temperate ice within polythermal glaciers is essential for understanding and modelling their dynamics. The boundary between both types of ice, termed as cold-temperate transition surface (CTS), is usually determined from ground-penetrating radar (GPR) data, given the permittivity contrast between cold ice and water-rich temperate ice. This task is traditionally manual and time-consuming. We here present an approach based on deep learning for the automatic classification of cold ice, temperate ice and bedrock. We used deep learning algorithms based on convolutional neural networks (CNN), following a feature pyramid network architecture. The training data were collected in Svalbard, using a GPR with central frequency of 20-25 MHz, along various campaigns spanning the period 2008-2022, carried out on glaciers in Sabine Land, Nordenskiöld Land, Wedel Jarlsberg Land and Nordaustlandet. To address data scarcity, we evaluated two dataset expansion strategies: generating synthetic radargrams by forward modelling of electromagnetic wave propagation, and a data augmentation scheme in which each GPR profile is split into 200 m segments treated as independent samples. Starting from a baseline trained on the original GPR dataset, these strategies were applied individually and in combination, defining four experiments. Our results show in general satisfactory values of the performance metrics. For instance, the intersection over union (IoU) metric reaches values of $64.2 \pm 2.7\%$, $77.0 \pm 2.4\%$ and $98.1 \pm 0.2\%$ for the classes cold ice, temperate ice and bedrock, respectively.

1 Introduction

Polythermal glaciers consist of both cold and temperate ice. The most studied type, the so-called Scandinavian-type polythermal glacier, consists of a basal layer of temperate ice overlain, in the accumulation zone, by the firn layer and, in the ablation zone, by a layer of cold ice, above which there is a surface layer up to 10-15 m in thickness that warms to the melting point seasonally (Cogley et al., 2010; Aschwanden et al., 2012). Polythermal glaciers are abundant in the High Arctic, in particular in the Canadian Arctic and the Svalbard archipelagos, and also in the sub-Antarctic islands. Some polythermal glaciers are

https://doi.org/10.5194/egusphere-2026-4083
Preprint. Discussion started: 21 July 2026

also found in mid-range elevation mountains in Scandinavia and in high-altitude mountains in temperate latitudes (Hambrey and Alean, 2004). The interest of their study lies in its two-layered structure, involving cold ice whose viscosity depends on temperature, and temperate ice whose viscosity depends on the fraction of liquid water content. This has an influence on ice deformation and therefore plays an important role in modelling the evolution of polythermal glaciers. A matter of particular interest is the evolution of the thermal structure of polythermal glaciers under a changing climate. Other characteristics of polythermal glaciers confer them additional interest. Among them, the fact that their mostly temperate base (in zones other than the terminus and the margins) implies much higher basal erosion rates than those of cold glaciers. They usually have a very thick basal debris load, up to half of the total thickness when approaching the snout; by contrast, the amount of debris carried in the surface is small. Regarding hydrological conditions, an important concern is to determine how meltwater flows through glaciers, because flow pathways control the response of glaciers to meteorological forcing, particularly with respect to meltwater outflow. (Hodgkins, 1997). In this sense, the meltwater runoff from polythermal glaciers follows patterns different from those typical of temperate glaciers. In the latter, most glacial meltwater reaches the bed, through crevasses and moulins, well before the snout, and normally emerges through a portal from a single subglacial water channel. In contrast, in polythermal glaciers meltwater cannot easily penetrate ice with subzero temperatures and tends to migrate towards the margins, creating two marginal water streams, or drains through surface channels towards the snout; therefore, a glacier portal is not formed. Finally, floating valley glacier tongues are mostly restricted to polythermal glaciers, as a temperate glacier terminus is usually too weak to float on water (Hambrey and Alean, 2004).

Radar methods have proved to be very useful in the investigation of polythermal glaciers. These methods involve the emission of electromagnetic waves and the detection of their subsurface reflections. Both airbone- and ground-based systems are commonly used in ice sheet and glacier investigations. Radar images provide critical information in glaciology: ice-bed interface, internal layering, snow/firn accumulation, crevasse delineation, among others (e.g. Dowdeswell and Evans, 2004; Navarro and Eisen, 2009). Airbone studies are mostly focused on great extension ice sheets, providing huge amounts of datasets used for studying ice sheet morphology, thickness, and dynamics from the air (MacGregor et al., 2021). Ground-penetrating radar (GPR) has been widely used to the study of the internal structure of glaciers (Watts and England, 1976; Benjumea et al., 2003; Navarro et al., 2005; Grabiec et al., 2011; Sold et al., 2013; Karušs et al., 2022). In the particular case of polythermal glaciers, GPR has been shown to be an essential tool for determining the englacial boundary between cold and temperate ice, known as the cold–temperate transition surface (CTS), because it constitutes a dielectric boundary between both types of ice. Therefore, it allows mapping the internal thermal structure of the glacier (Murray et al., 2000; Pettersson et al., 2003; Jania et al., 2005; Gusmeroli et al., 2012; Schannwell et al., 2014; Macheret et al., 2019; Letamendia et al., 2023; Kachniarz et al., 2025).

Traditionally, radar images have been interpreted using visual criteria by glaciologists. In particular, the CTS can be identified based on the differential radar reflectivity responses of cold and temperate ice. Cold ice is characterized by the absence of water, leading to the lack of internal reflections. Temperate ice, being at the melting point, does contain water which produces strong radar-wave scattering, revealed in the radargrams as a cloud of noise or diffractions due to the large contrast in dielectric properties between ice and water. Although glaciers contain various sources of scattering, such as debris content (Santin et al., 2023; Franke et al., 2023), water inclusions are considered the primary scatterers in temperate ice (Schannwell et al., 2014).

https://doi.org/10.5194/egusphere-2026-4083
Preprint. Discussion started: 21 July 2026

While Ogier et al. (2023) suggest that the characteristics of a temperate ice radargram cannot be reproduced in a synthetic dataset without the presence of water inclusions in the model, Franke et al. (2023) note that the reflection patterns of water inclusions and sediment particles with high dielectric properties are quite similar and thus their interpretation can be ambiguous.

Automating the procedures of radar image interpretation represents a major advancement, as glacier and ice sheet studies involve large amounts of radar data. Early works focused on automatic mapping of ice reflections using traditional techniques such as cross-correlation and pick-following methods (e.g. Fahnestock et al., 2001).

In recent years, there has been a growing interest in the application of machine-learning (ML) methods in geophysical image processing with the main purpose of facies classification or target detection. We will focus here in deep learning (DL) methods, i.e. ML methods using several computational layers. Deep learning (Lecun et al., 2015) based through Neural Networks (NNs) has emerged as the state-of-the-art approach across a wide range of disciplines, particularly in digital image processing and natural language processing (Vaswani et al., 2017; Krizhevsky et al., 2012). These models have demonstrated remarkable performance in tasks such as image classification, object detection, semantic segmentation, and language modelling. Neural networks are universal function approximators (Cybenko, 1989), constructed through the composition of fundamental building blocks. Each block typically consists of an affine transformation followed by a nonlinear activation function.

Supervised Deep learning involves the optimization (training) of the parameters of such networks using labelled datasets. The training process is formulated as the minimization of a loss function—commonly the Mean Squared Error (MSE) or cross-entropy—through gradient-based optimization techniques. The training of deep neural networks has led to significant advances in solving classical problems and has enabled the practical tackling of previously intractable challenges, thereby opening new frontiers in numerous scientific and engineering domains. However, the success of these models is highly dependent upon the quality, quantity, and accurate labelling of the training data. In the absence of sufficient and representative data, neural networks are prone to overfitting, which can severely impair their generalization capabilities on unseen data. The development of algorithms such as backpropagation (Rumelhart et al., 1986) and the advent of automatic differentiation frameworks have made it feasible to train deep networks with billions of parameters. These advances have been instrumental in scaling up model complexity and performance.

In the specific context of image processing tasks such as classification and segmentation, specialized architectures like Convolutional Neural Networks (CNNs) have been developed (Lecun et al., 1998). CNNs replace the dense matrix multiplications of traditional neural networks with convolution operations, thereby exploiting the local spatial correlations inherent in image data. In the study of glaciers and ice sheets using radar methods, DL techniques have been increasingly applied to analyze radargrams, particularly those obtained from airborne radar systems. Xu et al. (2018) and Kamangir et al. (2018) were the first to pursue the detection of the air-ice and ice-bedrock interfaces from airborne radar data using CNN combined with a recurrent neural network. A similar approach has been employed e.g. by Cai et al. (2020, 2021) and Dreier et al. (2025). DL techniques have also been applied to the detection of the snow layer and internal stratification within ice from airborne radar data (Rahnemoonfar et al., 2020; Ibikunle et al., 2020; Wang et al., 2021; Varshney et al., 2021; Moqadam et al., 2025).

For supervised methods such as CNN, a large enough amount of labelled data is required to obtain an optimum model. The use of synthetic datasets provides a way of obtaining true-labelled data that can be used for model training. Rahnemoonfar

https://doi.org/10.5194/egusphere-2026-4083
Preprint. Discussion started: 21 July 2026

et al. (2019) assessed the performance of ML-generated synthetic radar images to train a deep neuronal network. The authors concluded that synthetic radargrams failed to accurately replicate radar characteristics such as noise, suggesting that synthetic data alone should not be used to train a neural network to be applied to real data. Rahnemoonfar et al. (2020), in turn, noted the interest of further work exploring the training of the CNN using synthetic data which matches the noise and signal statistics of the actual radar data. Yari et al. (2021) generated synthetic airbone radar data using two different approaches: radar scattering physics with associated statistics and a conditional generative adversarial network. The comparision of both generated datasets highlighted the suitability of the physics simulator to obtain good structural characteristics, while the DL algorithm provided better textural signatures. Recently, Zhu et al. (2026) combined physics-based synthetic radargrams with transfer learning on field data to jointly extract internal layers and the ice-bedrock interface at Dome A (Antarctica).

To our knowledge, the transition between cold and temperate ice has not yet been studied using neural networks or machine learning approaches, which motivates the focus of the present paper. In particular, we aim to identify the CTS from radargrams acquired on polythermal glaciers. This will be supported by DL techniques. We will use a CNN trained using either real GPR data alone, synthetic data alone or a combination of both.

2 Data

In this work we use GPR data collected on various glaciers on the Svalbard archipelago during several field campaigns. We also use synthetic data with the aim of increasing the amount of data used to train the CNN algorithms for the classification of cold and temperate ice in radargrams from polythermal glaciers.

2.1 Field data

The ground-based radar measurements used in this work were taken in various campaigns in Svalbard between 2008 and 2022. The GPR surveys were carried out in Wedel Jarslberg Land, Sabine Land and Nordelskiöld Land in Spitsbergen, as well as the Austfonna Ice cap in Nordaustlandet. The details of the different surveys are summarized in Table 1. The layouts of the radar profiles are presented in Figure 1. The GPRs used were VIRL-6 (Berirkashvili et al., 2006) and VIRL-7 (Vasilenko et al., 2011), both with a central frequency of 20-25 MHz. The use of frequencies of this order allows a deep penetration, making possible the detection of the glacier bed, while also allowing the detection of the CTS. Figure 2 shows an example of a radargram with minimal processing, where the interface between cold and temperate ice can be observed. Most of these data have been used in previous studies, addressed to the calculation of the ice thickness and the volumes of cold and temperate ice (Martín-Espanol et al., 2013; Navarro et al., 2014, 2015; Lavrentiev et al., 2019; Macheret et al., 2019).

2.2 Synthetic data

To obtain a larger training dataset, we built a collection of synthetic radargrams using the open source program gprMax. This software numerically models the GPR signal propagation (Giannopoulos, 2005; Warren et al., 2016). Using the finite-difference approach in the time-domain FDTD (Kunz and Luebbers, 1993), gprMax applies Yee's algorithm to solve Maxwell's

https://doi.org/10.5194/egusphere-2026-4083
Preprint. Discussion started: 21 July 2026

Table 1. GPR surveys, with equipment used and its main characteristics, and total length of profiles.

Glacier	WGI* ID	Year	Radar	Frequency (MHz)	Sampling period (ns)	Profile (CTS) length (km)
Fridtjovbreen	NO4W01370000	2012	VIRL-6 and VIRL-7	20	2.5 and 5	180 (100)
Erdmannbreen	NO4W01370009	2012	VIRL-6	20	2.5	25 (19)
Recherchebreen	NO4W01310000	2011	VIRL-7	25	5	51
Tavlebreen	NO4W01360043	2010	VIRL-6 and VIRL-7	20	2.5	25 (2)
Grønfjordbreen	NO4W01410000	2010	VIRL-6	20	2.5	150 (66)
Elfenbeinbreen	NO4W01130000	2013	VIRL-7	25	5	105 (27)
Sveigbreen	NO4W01130008	2013, 2022	VIRL-7	25	5	72 (29)
Hansbreen	NO4W01240019	2009, 2016	VIRL-6 and VIRL-7	20	2.5 and 5	72 (20)
	NO4W02110006					
	NO4W02110007					
Austfonna	NO4W02110008	2008	VIRL-6	20	2.5	165 (13)
	NO4W02510005					
	NO4W02510006					

* WGI = World Glacier Inventory

equations in 2D or 3D. The algorithm provides significant flexibility in simulating a wide range of subsurface conditions, as it can effectively manage complex geometries and varied material configurations. To reduce computational cost we used the 2D modelling approach and the gprMax module for GPU (Warren et al., 2019).

We defined a polythermal glacier model by setting its geometry and the spatial distribution of the dielectric properties of its constituent materials. The geometry is common to all simulations: 150 m (vertical) $\times$ 200 m (horizontal). The uppermost 2 m consist of air, underlain by a 4-m layer of snow, followed by the ice layer and 10 m of bedrock thickness at the bottom. The ice-bedrock interface can be either flat or slightly undulating. The polythermal structure results from defining cold and temperate ice layers, whose ice is characterised by the same dielectric properties but the latter layer includes water inclusions within it. Table 2 shows the dielectric properties of the different materials used. The water inclusions in the temperate ice are macroscopic diffractors with a randomly variable radius between the model discretisation size (0.05 m) and a maximum radius, which varies between 0.10 and 0.15 m. The amount and maximum radius of diffractors for a particular simulation is defined so that the average liquid water content (LWC) reaches a typical value of temperate ice of 0.2% (Bradford and Harper, 2005; Ogier et al., 2023). While the sizes and amount of water inclusions differ from reality, the wavelength of the radar signal is in the order of a few metres, which is much larger than the size of the inclusions, and thus represents an integral over the wavelength of the dielectric properties of the medium. We defined the shape of the CTS as sum of a linear function plus a sinusoidal component, whose parameters are selected randomly, resulting in distinct shapes for different simulations.

In order to obtain more complex synthetic radargrams, we added different elements to the model. Firstly, we randomly included in the ice circular bodies representing water pockets or cross-sections of air- or water-filled channels. The radius of

https://doi.org/10.5194/egusphere-2026-4083
Preprint. Discussion started: 21 July 2026

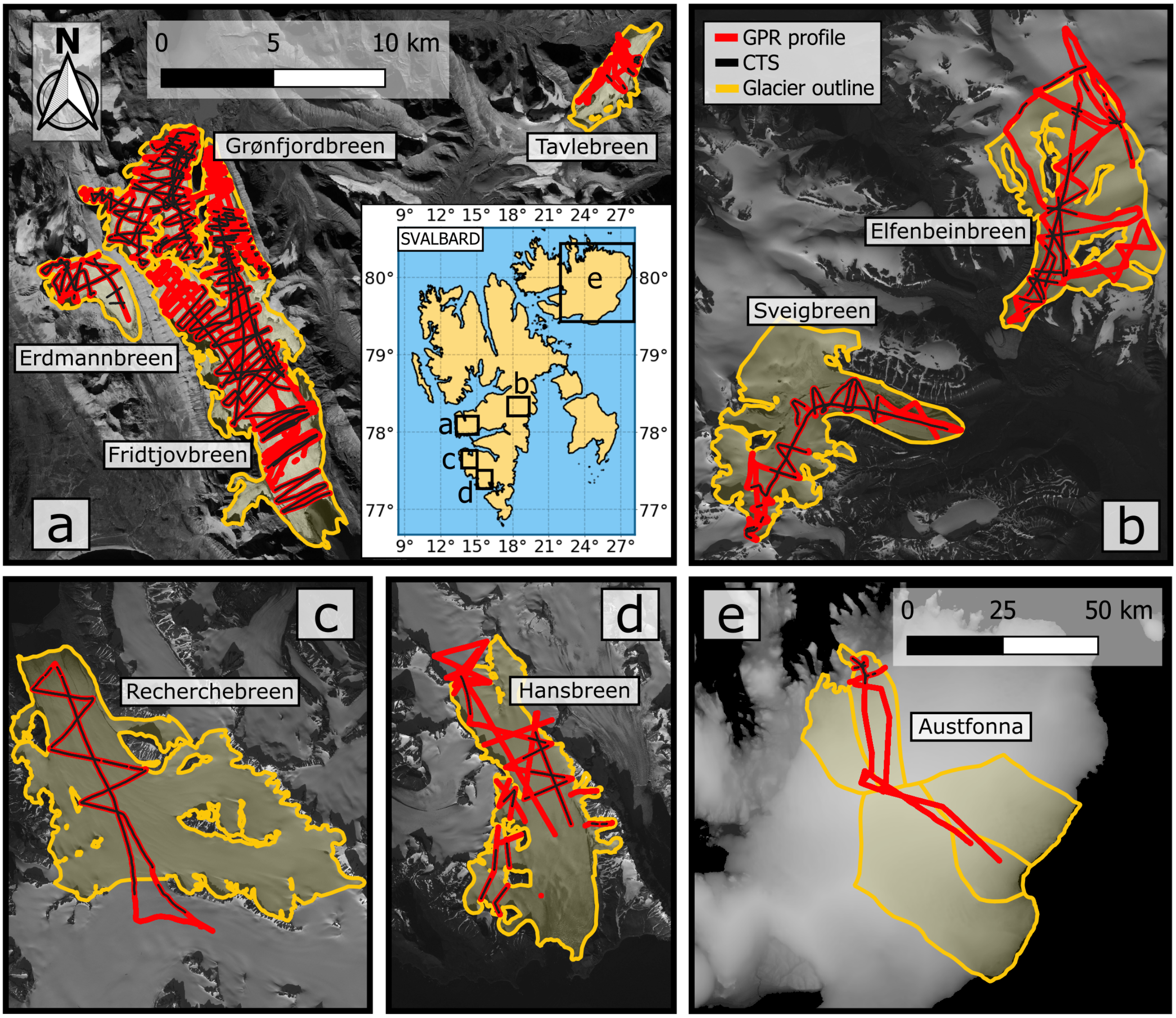

Figure 1. Layout of the radar profiles on the studied glaciers. The black lines indicate sections of the profiles where a temperate ice layer was clearly identified. The glacier outlines correspond to RGI V7 (RGI Consortium, 2023). Panels b, c and d share the scale used in panel a. The inset shows the location of the various study zones within Svalbard. The satellite image used as background in panel a contains modified Copernicus Sentinel data of 2020, while that in panels b, c and d was available from ASTER (Advanced Spaceborne Thermal Emission and Reflection Radiometer) ©METI (Ministry of Economy, Trade and Industry, Japan) and NASA (US National Aeronautics and Space Administration) (2005), for 23 July 2005 (all rights reserved), courtesy of the University of Silesia, Poland, within the frame of cooperation of the PolarClimate-SvalGlac project, and panel e is from Moholdt et al. (2019).

https://doi.org/10.5194/egusphere-2026-4083
Preprint. Discussion started: 21 July 2026

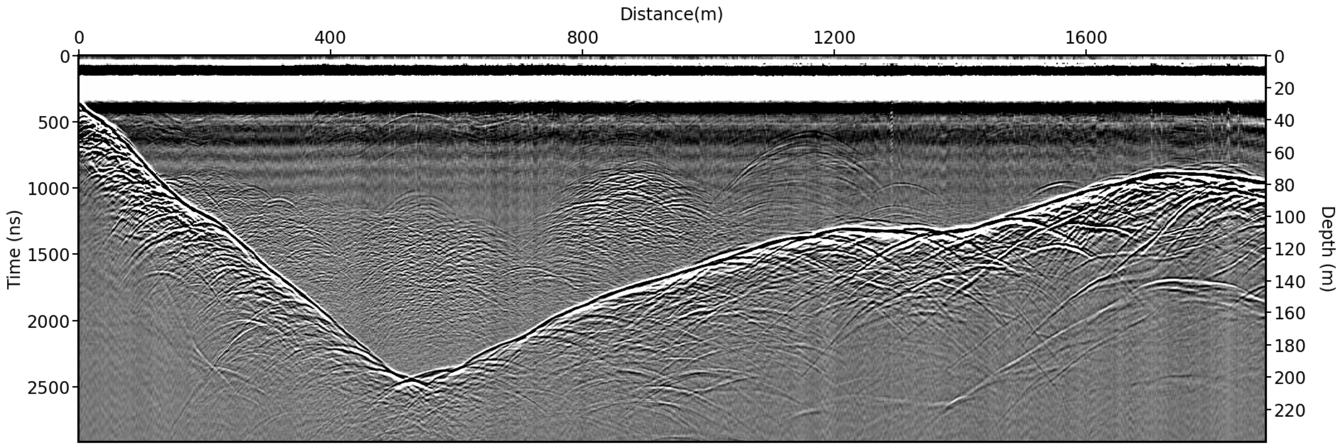

Figure 2. Radargram of 25 MHz GPR profile registered on Sveigbreen in 2022. The depth scale was estimated using a radio wave velocity of 168 m μs^{-1}.

these bodies varied between 0 and 1 m. Another element that we incorporated was surface crevasses. These were simulated as openings at the surface with a width of 0.6 m that gradually narrows, reaching depths down to 8 m. These crevasses can be partially water-filled or water-free. Other elements we included were internal fractures or small elongated cavities. These elements are defined in the model as segments whose orientation, length and width vary randomly within a given range, and can contain air or water. Figure 3 shows an example of synthetic polythermal glacier model and its associated radargram.

The source signal was configured as a Hertzian dipole with a Ricker-type source-time function and a dominant frequency coincident with that of real antennas used in our field campaigns (ca. 25 MHz). The position of the antennas in our model is just above the surface. We have set the separation between antennas at a constant distance of 7 m, in agreement with the typical values used for the acquisition of our Svalbard GPR dataset. The spacing between traces is constant at 0.5 m. Each profile consists of a total of 380 traces, thus covering a profile length of 190 m. The discretisation size Δl of the model was chosen as a trade-off between avoiding numerical dispersion and setting a reasonable cell size in terms of computational cost. To avoid numerical dispersion in gprMax, $\Delta l \leq \lambda_{\min}/10$ must be satisfied (Warren et al., 2016). In our case, the smallest wavelength corresponds to water ($\lambda_{\min} = 0.44$ m; Ogier et al., 2023), which is the material with the highest permittivity. This resulted in the choice of $\Delta l = 0.05$ m. Table 3 summarizes the set of parameters used for numerical modelling in gprMax.

3 Methodology

3.1 Data treatment

The processing of radar data was minimal, with only time-zero correction and trimming of the time window. Bandpass filtering was applied exclusively to facilitate data interpretation and was not applied to the training, validation, or test sets. Synthetic data has not been processed for interpretation. The delineation of the CTS was done manually, identifying this interface as

https://doi.org/10.5194/egusphere-2026-4083
Preprint. Discussion started: 21 July 2026

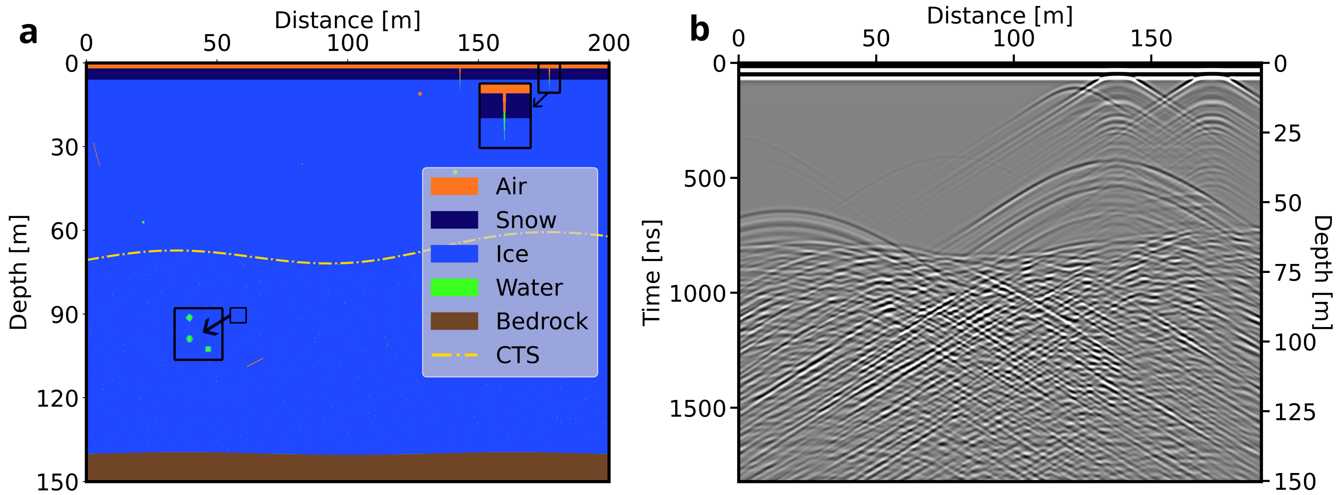

Figure 3. (a) Geometry of a polythermal glacier model with its different constituent materials. The ice matrix of cold and temperate ice share similar dielectric properties, but the latter contains inclusions of liquid water. The top zoom shows a superficial crevasse partially filled with water, and the other shows macroscopic water inclusions in the temperate ice. (b) Synthetic radargram of the model shown in (a), generated using gprMax.

Table 2. Dielectric propierties of the materials used in the gprMax simulations.

Material	Permittivity ε_r	Conductivity σ (S m^{-1})
Air	1	0
Snow	1.8	2.5×10^{-5}
Ice	3.17	5×10^{-8}
Water	80	5×10^{-4}
Bedrock	8	1×10^{-3}

Dielectric properties of bedrock (limestone and shale) and water are taken from Davis and Annan (1989) and those of ice from Evans (1965) and Plewes and Hubbard (2001). Dielectric properties of snow are calculated from Bogorodsky et al. (1985) and Granlund et al. (2010) with a snow density of ρ_{snow} = 400 kg m^{-3} and LWC = 0.5%, which are values of dry snow.

the boundary between an area transparent to radar energy (identified as cold ice) and an area characterized by a high level of backscattered radar energy (identified as temperate ice) (e.g. Pettersson et al., 2004; Gusmeroli et al., 2012; Letamendia et al., 2023). Both data processing and interpretation (i.e. picking) were carried out using ReflexW commercial software (Sandmeier, 2024). Data segmentation consisted in classifying the image content into three classes: cold ice, temperate ice and bedrock. The original data were first normalised to values between 0 and 1, and then resized by downsampling to 256 $\times$ 256 pixels.

https://doi.org/10.5194/egusphere-2026-4083
Preprint. Discussion started: 21 July 2026

Table 3. gprMax model parameters.

gprMax parameters	Value
Frequency	25 MHz
Waveform type	Ricker
Antenna dipole	Hertzian
Antenna separation	7 m
Trace spacing	0.5 m
Domain (x, y, z)	200, 150, 0.05 m
Cell size	0.05 m
Time window	2×10^{-6} s
Time step	1.18×10^{-10} s

3.2 Deep Learning algorithm

In this work, we approach the ice segmentation problem using a Fully Convolutional Network (FCN) (Long et al., 2015). This framework allows a pixel-wise classification of images with arbitrary sizes while reducing the number of parameters of the model by avoiding fully connected layers. In particular, to classify as cold ice, temperate ice and bedrock in a context of varying spatial scales inherently related to the data acquisition process, we implement and train a Feature Pyramid Network (FPN) (Lin et al., 2017). In contrast to FCNs, the FPN architecture employs a top-down pathway with lateral connections (Fig. 4). This mechanism merges semantic information from deep layers with spatial details from earlier layers to recover resolution.

The bottom-up pathway, the first part of the FPN architecture, is the feed-forward computation of the network. In this case, we use ResNet-34 as the backbone of our model (He et al., 2015). This pathway is the encoder of the network and is the part that extracts the features from the input data, generating feature maps. Within this pathway the encoder has 5 sub-sampling steps, and the feature outputs of the last residual block of ResNet-34 at each stage are used (C2, C3, C4 and C5 in Fig. 4). In the top-down pathway, the resolution is restored by upsampling steps. The corresponding feature maps are semantically stronger. These features are enriched by lateral connections with their corresponding bottom-up level, which are semantically weaker. However, as they were subsampled fewer times, the activations are more precisely localised. This lateral connection consists of a 1×1 convolution layer of the bottom-up level and an element-wise addition with the upsampled map. Predictions are made at each top-down level (P2, P3, P4 and P5) and then upsampled to the original input size and concatenated. Finally, a segmentation head creates a probability map with the 3-class prediction. The class assigned to each pixel corresponds to the highest probability value, obtained by applying an argmax operation.

This configuration is particularly appropriate for this study, as it preserves the boundary precision required to distinguish between adjacent cold and temperate ice regions. To train the neural network, we use a cross-entropy-loss cost function. The hyper-parameters characterising our training scheme are given in Table 4.

https://doi.org/10.5194/egusphere-2026-4083
Preprint. Discussion started: 21 July 2026

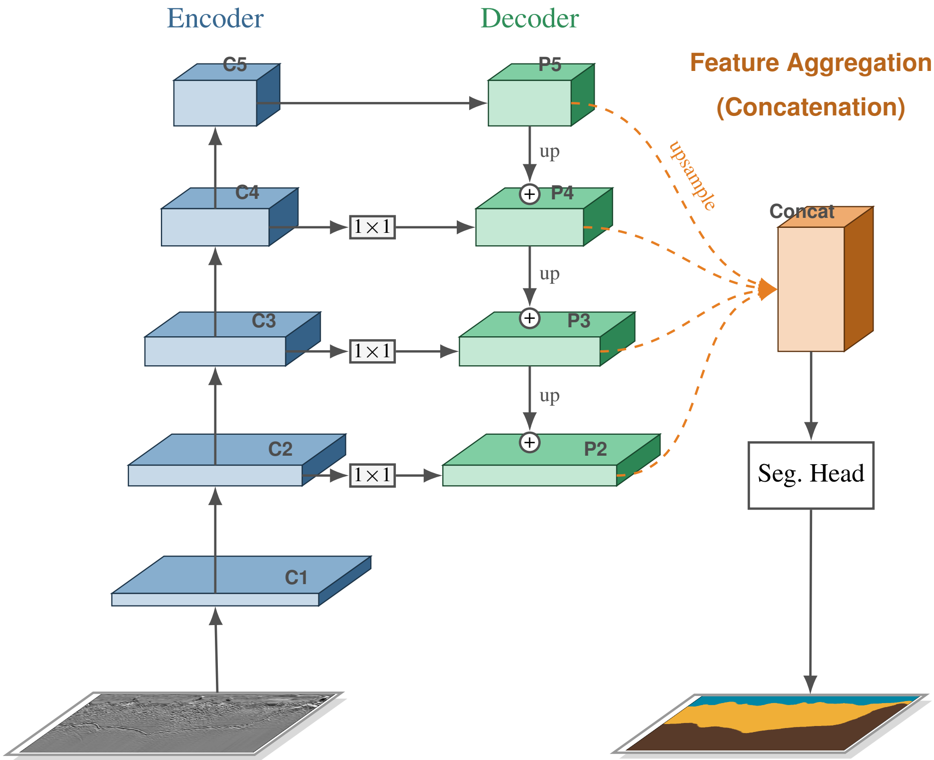

Figure 4. Overview of the proposed Feature Pyramid Network (FPN) architecture for ice segmentation. The model utilizes a top-down pathway with lateral connections to merge high-level semantic information with low-level spatial details.

3.3 Model training and cross-validation

Our dataset shows large differences between campaigns and glaciers. Additionally, radargrams from the same campaign and glacier show similarities in characteristics such as background noise, ringing, or the ease/difficulty of distinguishing the CTS. For these reasons, we have trained the model following a cross-validation scheme by glacier and campaign. For the test, we chose GPR profiles collected on Fridtjovbreen in 2012. These profiles include a balance of easily interpretable features and more complex settings, characterised by artefacts and noise. The testing subset also contains data obtained using two different GPR systems (VIRL-6 and VIRL-7) and represents approximately 20% of the total profiles in the dataset. Additionally, the test set corresponds to a campaign entirely unseen by the model, thus allowing for a more accurate assessment of its generalisation capabilities, while preventing information leakage across campaigns.

The training dataset consists of ten distinct glacier-campaign sets. Accordingly, ten training runs were performed, each using a different glacier-campaign set as the validation set, and the remaining nine for training. This procedure was followed regardless of the number of profiles in the validation set. For each training run, the Intersection over Union (IoU) of the validation set was monitored, and the best-performing model was selected. This results in avoiding overfitting.

https://doi.org/10.5194/egusphere-2026-4083
Preprint. Discussion started: 21 July 2026

Table 4. Network hyperparameters and training configuration.

Hyperparameter	Value	Comment
Number of layers	34	The backbone is ResNet-34 (He et al., 2015).
Trainable parameters	23.1 M	Weights of the network that can be learned during training.
Pre-trained weights	ImageNet	The training was performed using pre-trained values with the ImageNet dataset (Krizhevsky et al., 2012), which contains more than 14 million images. This technique is known as transfer learning.
Learning rate	1×10^{-3}	Step size of the optimisation algorithm for adjusting the model parameters.
Epochs	100	Each pass across the whole training set.
Batch size	8	Number of samples used simultaneously to compute weight updates.
Optimiser	Adam	Algorithm that refines model parameters via gradient-based updates to reduce the loss (Kingma and Ba, 2017).
Weight decay	1×10^{-5}	Regularizaton technique based on L_2 norm to prevent overfitting.

In total, four experiments were conducted. Experiment 1 uses exclusively the GPR measurements dataset described in Section 2.1. Experiment 2 builds on this setup by incorporating the synthetic dataset as additional training data. Experiment 3 applies the same configuration as Experiment 1, but introduces an additional pre-processing step on the GPR measurements. Specifically, each profile is subdivided into segments of 200 m, which are treated as independent samples to increase the size of the training set. Experiment 4 follows the same approach as Experiment 2, also including this pre-processing step. As in Experiment 3, the GPR profiles are split into 200 m segments, which serve as a data augmentation strategy. This size was selected in accordance with the size of the synthetic radargrams. Given that, before being fed into the network, each radargram is downsampled to 256×256 pixels, this procedure allows us to extract more information from each radargram. We additionally tested other augmentation techniques, such as random horizontal flips and the addition of Gaussian noise. These strategies did not produce any discernible improvement, so their results were not considered.

4 Results

To evaluate the performance of models in semantic segmentation, metrics based on a confusion matrix are commonly used. This matrix measures the accuracy of the model in a class defined as positive over the rest of the classes. For each class, it measures the number of true positives (TP), false positives (FP), true negatives (TN) and false negatives (FN) obtained. We evaluated the model's performance on the test set using four common semantic segmentation metrics shown below:

https://doi.org/10.5194/egusphere-2026-4083
Preprint. Discussion started: 21 July 2026

– IoU: $\frac{TP}{TP+FP+FN}$

– Precision: $\frac{TP}{TP+FP}$

– Recall: $\frac{TP}{TP+FN}$

– F1 score: $2\frac{Precision \cdot Recall}{Precsion+Recall} = \frac{2TP}{2TP+FP+FN}$

The above metrics were applied to each of the experiments described in section 3.3. Table 5 shows the evaluation results for each of the classes in the test set. These results represent the average of training the model with five different weight initialisations, together with their standard deviation.

Table 5. Overview of model performance, expressed as percentage, in the four experiments conducted, using various metrics for each of the classes in the test set (cold ice, temperate ice and bedrock). For each experiment, the training dataset used and the number of radargrams (samples) involved are given. The results are the average of five training sessions with different weight initializations; their standard deviation is also given. For each metric and class, the highest value with low standard deviation of the metric among all experiments is boldfaced.

n=5 trainings	Training data (size)	Metrics	Cold ice (mean $\pm\sigma$)	Temperate ice (mean $\pm\sigma$)	Bedrock (mean $\pm\sigma$)
Experiment 1	GPR dataset	IoU	63.5 ± 2.5	74.0 ± 2.8	98.2 ± 0.4
	(138 samples)	F1 Score	77.4 ± 1.9	85.0 ± 1.9	99.1 ± 0.2
		Precision	67.3 ± 2.6	$\mathbf{92.9 \pm 0.9}$	99.4 ± 0.1
		Recall	91.1 ± 1.0	78.4 ± 2.7	98.7 ± 0.3
Experiment 2	GPR dataset	IoU	65.0 ± 5.1	74.8 ± 6.1	$\mathbf{98.5 \pm 0.1}$
	+ synthetic dataset	F1 Score	78.6 ± 3.9	85.5 ± 4.1	$\mathbf{99.3 \pm 0.1}$
	(230 samples)	Precision	69.1 ± 6.3	93.6 ± 3.9	$\mathbf{99.5 \pm 0.1}$
		Recall	$\mathbf{91.8 \pm 1.2}$	78.9 ± 6.8	$\mathbf{99.1 \pm 0.2}$
Experiment 3	GPR dataset	IoU	57.1 ± 8.6	67.4 ± 15.7	96.6 ± 1.8
	split every 200 m	F1 Score	72.3 ± 7.3	79.3 ± 13.0	98.3 ± 0.9
	(1583 samples)	Precision	61.6 ± 10.0	92.1 ± 0.9	98.3 ± 0.2
		Recall	89.3 ± 15.6	71.7 ± 17.2	98.3 ± 0.5
Experiment 4	GPR dataset	IoU	$\mathbf{64.2 \pm 2.7}$	$\mathbf{77.0 \pm 2.4}$	98.1 ± 0.2
	split every 200 m	F1 Score	$\mathbf{78.2 \pm 2.0}$	$\mathbf{87.0 \pm 1.5}$	99.0 ± 0.1
	+ synthetic dataset	Precision	$\mathbf{68.9 \pm 3.2}$	93.6 ± 3.9	99.3 ± 0.2
	(1668 samples)	Recall	90.6 ± 1.4	$\mathbf{81.2 \pm 2.6}$	98.8 ± 0.3

5 Discussion

According to Table 5, the best classification performance is achieved in Experiment 4. For the cold ice and temperate ice classes, the best results considering the whole set of metrics are obtained in this experiment. Regarding the bedrock class, values greater

https://doi.org/10.5194/egusphere-2026-4083
Preprint. Discussion started: 21 July 2026

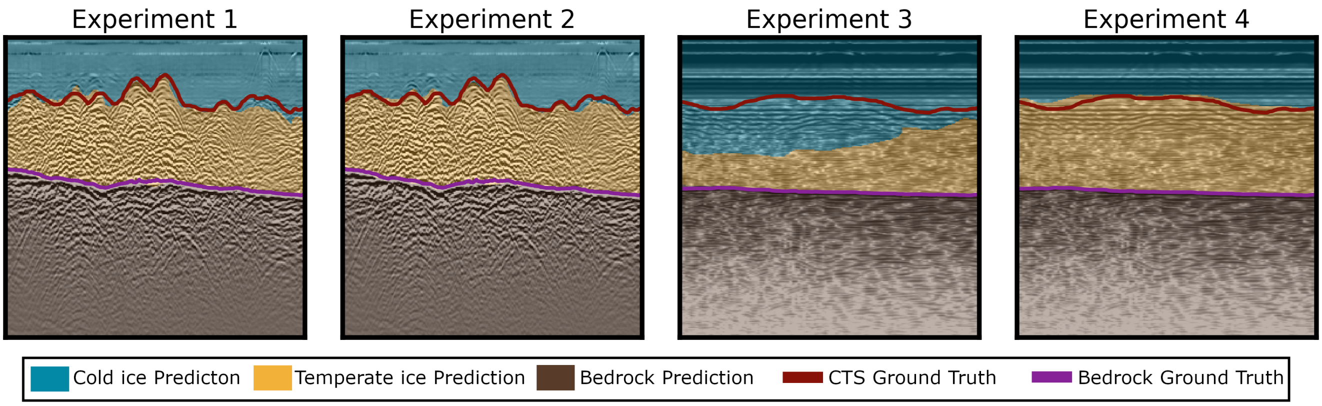

Figure 5. Prediction results of the four experiments on a test-set radargram. Experiments 1 and 2 use the complete radargram, whereas Experiments 3 and 4 use a subsection of it. The radargram is shown as background.

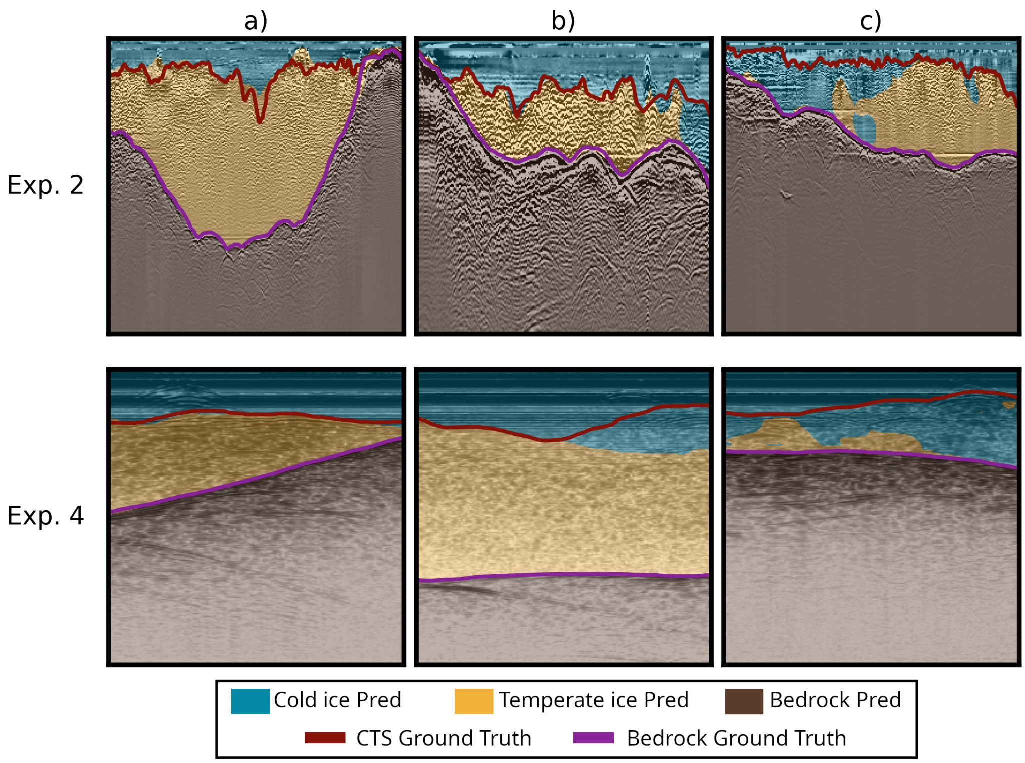

Figure 6. A sample of prediction results of experiments 2 and 4 illustrating a good performance (a), moderate misclassification (b) and poor classification (c).

https://doi.org/10.5194/egusphere-2026-4083
Preprint. Discussion started: 21 July 2026

than 98% are achieved in all metrics, showing that the model is able to classify the bedrock very accurately. The differences between experiments for this class are negligible and fall within the run-to-run variability. Although Experiment 4 does not produce the highest scores for the bedrock class, it provides the best overall classification performance when considering all classes. However, the improvement in results compared with Experiments 1 and 2 is not significant, as it falls within the range of variability between training runs.

Comparing the two experiments trained only with real data (Experiments 1 and 3) shows that splitting the radargrams into 200 m segments does not improve the classification of the ice classes: the mean IoU of both the cold and temperate ice classes is lower in Experiment 3 than in Experiment 1 and the standard deviation increases significantly (e.g. for the temperate ice IoU metric, it rises from 2.8% to 15.7%). This data augmentation strategy increases the number of training samples but introduces a training instability when applied to the real dataset alone.

The effect of adding synthetic radargrams to the GPR dataset depends on the experiment setup strategy. Comparing Experiments 1 and 2 (i.e., those without radargram segmentation), the addition of synthetic data produces only a minimum change in the mean values of the ice class metrics, accompanied by a slight increase in their dispersion. Comparing experiments 3 and 4, in which segmented radargrams have been used, the addition of synthetic data has a substantial effect: in cold and temperate ice classes the IoU increases approximately 7 and 10 percentage points, respectively, and their standard deviation decrease from 8.6% and 15.7% to 2.7% and 2.4%. The addition of synthetic radargrams removes the instability observed in Experiment 3. An example is provided by Figure 5, which evidences the best model performance of Experiment 4 compared with 3.

In all experiments the amount of cold ice is slightly overpredicted, implying an under-prediction of temperate ice. This is in agreement with the high recall value and the low precision value given in Table 5 for the cold ice class. Note, in the definition of the metrics, that the recall includes the number of false negatives in the denominator, while the precision includes the number of false positives. This pattern reflects the ambiguity of the CTS location. In spite of the slightly better overall performance of experiments 2 and 4, there are cases in which misclassification occurs, as shown in Figure 6.

The above paragraphs suggest that the approach of expanding the training dataset using synthetic data does not significantly improve the performance of the model, although it notably reduces the standard deviation when passing from Experiment 3 to 4. This, considered together with the high computational cost of generating synthetic radargrams, makes this approach unattractive. Nevertheless, we acknowledge the usefulness of synthetic radargrams for interpreting the internal structure of polythermal glaciers, particularly given the scarcity of ground-truth information regarding the internal structure of glaciers. By providing a direct link between a controlled subsurface model and its corresponding GPR response, synthetic radargrams offer valuable insight that can improve the interpretation of observed radar reflections.

Overall, across the four experiments, classification errors mostly correspond to the cold and temperate ice classes rather than to the bedrock class. The bedrock class is easily distinguishable in the feature space learned by the network, as its signature in GPR data is more characteristic than that of cold and temperate ice, and the ice-bedrock transition is usually very marked. The cold–temperate ice transition is generally more gradual and less clearly defined. Moreover, the human interpretation involved in the ground truth also carries an inherent uncertainty due to its subjective nature, which can entail biases.

https://doi.org/10.5194/egusphere-2026-4083
Preprint. Discussion started: 21 July 2026

It is important to keep in mind that we are using as ground truth a human-delineated CTS. Due to the diffuse boundary between the cold and temperate ice layers, this necessarily involves interpretation errors. These can be reduced following a technique such as that used by Gusmeroli (2010) or Letamendia et al. (2023) whereby several sets of pickings of the CTS are performed by different researchers. A further difficulty of classification models, such as the one described in this paper, is that they do not consider the impact of debris on GPR data. Debris located near the base of the glacier can generate scattering signatures similar to those produced by water inclusions (Franke et al., 2023), which can lead to an overestimation of the amount of temperate ice. However, given the limited evidence available to reliably incorporate debris-related signatures into the interpretation, such an analysis was not considered in the present study.

Regarding the uncertainty introduced by the pixel size, the input radargrams were downsampled from their original temporal resolution to 256 pixels along the time axis. The mean time window across the dataset was approximately 4,400 ns, and sampling intervals ranging from 2.5 to 5 ns depending on the GPR system were employed. Converting to ice thickness using a constant radio-wave velocity of 168 m μs^{-1}, the uncertainty introduced by the pixel size corresponds to a mean depth uncertainty of approximately 1.4 m. This uncertainty falls within the vertical resolution of the GPR system, which is theoretically defined as $\lambda/4$ (being λ the dominant wavelength), but in practice can reach $\lambda/2$ (Navarro and Eisen, 2009). For a central frequency of 25 MHz, the theoretical vertical resolution thus ranges between 1.6 m and 3.3 m.

For training the model we used raw GPR data, without any processing, with the aim of minimizing the removal of potential information relevant for classification. In practice, we only applied time-zero correction and time-window trimming to focus on the radar section of interest. The presence of temperate ice is mainly identified through the presence of high back-scattering and hyperbolic diffractions. To avoid suppressing hyperbolae, no migration was applied, thus preserving the characteristic response of temperate ice and avoiding the assumption of a constant propagation velocity within each radargram.

6 Conclusions and outlook

From the above analysis, the following main conclusions can be drawn:

1. CNN-based methods have been shown to be a useful tool for identifying the electromagnetic signature of cold and temperate ice, and thus for determining their spatial distribution in polythermal glaciers.

2. Increasing the size of the training dataset by using synthetic data does not result in a significant improvement of the model performance. More detailed simulations, capable of capturing fine-scale noise patterns, would be required to make the use of synthetic data useful. In any case, the expected high computational cost could be a significant drawback. Even so, synthetic radargrams are a helpful tool for interpreting the internal structure of polythermal glaciers.

3. Data augmentation strategies based on fragmentation of the original radargrams into smaller sections significantly increase the standard deviation between training runs. When combined with synthetic data the results improve slightly. Therefore, interpretation based on global features appears to be more effective than exploiting small-scale phenomena.

4. The best classification results are obtained for the bedrock class, given the higher contrast in electric properties between bed and glacier ice compared to those between cold and temperate ice.

Future studies of interest could include the use of data collected using a variety of GPR systems and frequencies, to obtain a more robust classification model. Another matter of interest would be the discrimination of the electromagnetic response of ice with debris inclusions versus the response of temperate ice. This would prevent a possible misinterpretation of the temperate ice class.

Code and data availability. The dataset is available at https://doi.org/10.5281/zenodo.21134524 (Letamendia et al., 2026), and the implementation at https://doi.org/10.5281/zenodo.21260762 (Letamendia and Ramírez, 2026) or https://github.com/unailetamendia/DL-GPR-polyglaciers.git

Author contributions. Conceptualization: UL, FN, BB (general aspects), IR, ES (CNN aspects). Code writing and implementation: UL. Data collection: FN and IL. Data processing and interpretation: UL. Manuscript writing: UL, FN, BB and IR. Manuscript review: UL, FN, BB, IR and ES.

Competing interests. The authors declare no competing interests.

Acknowledgements. This research was funded by grants PID2020-113051RB-C31 (GLACEVOL), PID2021-123825OB-I00 (ALGEMAR) and PID2024-158484NB-I00 (DINGLAC) from MCIN / AEI / 10.13039 / 501100011033 / FEDER, UE, as well as the European Union's Horizon Europe research and innovation programme through the project LIQUIDICE (grant number: 101184962). UL was supported by grant PRE2021-100049 financed by MCIN/AEI/10.13039/501100011033 and by FSE+. IL was supported by State Assignment No 2024-0004 of the IGRAS.

In order to check for grammatical or spelling errors the authors have used Claude (https://claude.ai/, last access: 6 July 2026) and DeepL (https://www.deepl.com/es/translator, last access: 6 July 2026).

https://doi.org/10.5194/egusphere-2026-4083
Preprint. Discussion started: 21 July 2026

References

Aschwanden, A., Bueler, E., Khroulev, C., and Blatter, H.: An enthalpy formulation for glaciers and ice sheets, Journal of Glaciology, 58, 441–457, https://doi.org/10.3189/2012JoG11J088, 2012.

Benjumea, B., Macheret, Y. Y., Navarro, F. J., and Teixidó, T.: Estimation of water content in a temperate glacier from radar and seismic sounding data, Annals of Glaciology, 37, 317–324, https://doi.org/10.3189/172756403781815924, 2003.

Berirkashvili, V. S., Vasilenko, E. V., Macheret, Y. Y., and Sokolov, V. G.: Ul'sny radar dlya zondirovaniya lednikov s opticheskim kanalom sinkhronizatsii i tifrovoy brabotkoy signalov [Monopulse radar for sounding of glaciers with optical synchronization channel and digital processing of signals], Radiotekhnika, 9, 52–57, 2006.

Bogorodsky, V. v., Bentley, C. R., and Gudmandsen, P. E.: Radioglaciology, D. Reidel Publishing Company, 1 edn., ISBN 978-94-010-8830-5, 1985.

Bradford, J. H. and Harper, J. T.: Wave field migration as a tool for estimating spatially continuous radar velocity and water content in glaciers, Geophysical Research Letters, 32, https://doi.org/10.1029/2004GL021770, _eprint: https://onlinelibrary.wiley.com/doi/pdf/10.1029/2004GL021770, 2005.

Cai, Y., Hu, S., Lang, S., Guo, Y., and Liu, J.: End-to-End Classification Network for Ice Sheet Subsurface Targets in Radar Imagery, Applied Sciences, 10, 2501, https://doi.org/10.3390/app10072501, number: 7, 2020.

Cai, Y., Liu, D., Xie, J., Yang, J., Cui, X., and Lang, S.: Attention Multi-Scale Network for Automatic Layer Extraction of Ice Radar Topological Sequences, Remote Sensing, 13, 2425, https://doi.org/10.3390/rs13122425, number: 12, 2021.

Cogley, J. G., Hock, R., Rasmussen, L. A., Arendt, A. A., Bauder, A., Braithwaite, R. J., Jansson, P., Kaser, G., Moller, M., Nicholson, L., and Zemp, M.: Glossary of glacier mass balance and related terms, International Hydrological Programme, 86, 2010.

Cybenko, G.: Approximation by superpositions of a sigmoidal function, Mathematics of Control, Signals and Systems, 2, 303–314, https://doi.org/10.1007/BF02551274, 1989.

Davis, J. L. and Annan, A. P.: Ground-Penetrating Radar for High-Resolution Mapping of Soil and Rock Stratigraphy, Geophysical Prospecting, 37, 531–551, https://doi.org/10.1111/j.1365-2478.1989.tb02221.x, _eprint: https://onlinelibrary.wiley.com/doi/pdf/10.1111/j.1365-2478.1989.tb02221.x, 1989.

Dowdeswell, J. A. and Evans, S.: Investigations of the form and flow of ice sheets and glaciers using radio-echo sounding, Reports on Progress in Physics, 67, 1821–1861, https://doi.org/10.1088/0034-4885/67/10/R03, 2004.

Dreier, M., Koch, M., Gourmelon, N., Blindow, N., Steinhage, D., Wu, F., Seehaus, T., Braun, M., Maier, A., and Christlein, V.: IceAnatomy: a benchmark dataset and methodology for automatic ice boundary extraction from radio-echo sounding data, The Cryosphere, 19, 5337–5359, https://doi.org/10.5194/tc-19-5337-2025, 2025.

Evans, S.: Dielectric Properties of Ice and Snow–a Review, Journal of Glaciology, 5, 773–792, https://doi.org/10.3189/S0022143000018840, 1965.

Fahnestock, M., Abdalati, W., Luo, S., and Gogineni, S.: Internal layer tracing and age-depth-accumulation relationships for the northern Greenland ice sheet, Journal of Geophysical Research: Atmospheres, 106, 33 789–33 797, https://doi.org/10.1029/2001JD900200, _eprint: https://onlinelibrary.wiley.com/doi/pdf/10.1029/2001JD900200, 2001.

Franke, S., Gerber, T., Warren, C., Jansen, D., Eisen, O., and Dahl-Jensen, D.: Investigating the Radar Response of Englacial Debris Entrained Basal Ice Units in East Antarctica Using Electromagnetic Forward Modeling, IEEE Transactions on Geoscience and Remote Sensing, 61,

https://doi.org/10.5194/egusphere-2026-4083
Preprint. Discussion started: 21 July 2026

4301 516, https://doi.org/10.1109/TGRS.2023.3277874, num Pages: 16 Place: Piscataway Web of Science ID: WOS:001005737500027, 2023.

Giannopoulos, A.: Modelling ground penetrating radar by GprMax, Construction and Building Materials, 19, 755–762, https://doi.org/10.1016/j.conbuildmat.2005.06.007, 2005.

Grabiec, M., Puczko, D., Budzik, T., and Gajek, G.: Snow distribution patterns on Svalbard glaciers derived from radio-echo soundings, Polish Polar Research, 32, 393–421, https://doi.org/10.2478/v10183-011-0026-4, 2011.

Granlund, N., Lundberg, A., and Gustafsson, D.: Laboratory study of the influence of salinity on the relationship between electrical conductivity and wetness of snow, Hydrological Processes, 24, 1981–1984, https://doi.org/10.1002/hyp.7659, _eprint: https://onlinelibrary.wiley.com/doi/pdf/10.1002/hyp.7659, 2010.

Gusmeroli, A.: Polythermal glacier dynamics at Storglaciaren, Arctic Sweden, inferred using in situ geophysical techniques, Ph.D. thesis, Swansea University, https://cronfa.swan.ac.uk/Record/cronfa42751/Details, 2010.

Gusmeroli, A., Jansson, P., Pettersson, R., and Murray, T.: Twenty years of cold surface layer thinning at Storglaciären, sub-Arctic Sweden, 1989-2009, Journal of Glaciology, 58, 3–10, https://doi.org/10.3189/2012JoG11J018, 2012.

Hambrey, M. and Alean, J.: Glaciers, Cambridge University Press, Cambridge, 2 edn., https://doi.org/10.1017/CBO9780511807602, 2004.

He, K., Zhang, X., Ren, S., and Sun, J.: Deep Residual Learning for Image Recognition, https://doi.org/10.48550/arXiv.1512.03385, arXiv:1512.03385 [cs], 2015.

Hodgkins, R.: Glacier hydrology in Svalbard, Norwegian high arctic, Quaternary Science Reviews, 16, 957–973, https://doi.org/10.1016/S0277-3791(97)00032-2, 1997.

Ibikunle, O., Paden, J., Rahnemoonfar, M., Crandall, D., and Yari, M.: Snow Radar Layer Tracking Using Iterative Neural Network Approach, in: IGARSS 2020 - 2020 IEEE International Geoscience and Remote Sensing Symposium, pp. 2960–2963, ISSN 2153-7003, https://doi.org/10.1109/IGARSS39084.2020.9323957, 2020.

Jania, J., Macheret, Y. Y., Navarro, F. J., Glazovsky, A. F., Vasilenko, E. V., Lapazaran, J., Glowacki, P., Migala, K., Balut, A., and Piwowar, B. A.: Temporal changes in the radiophysical properties of a polythermal glacier in Spitsbergen, Annals of Glaciology, 42, 125–134, https://doi.org/10.3189/172756405781812754, 2005.

Kachniarz, K., Grabiec, M., Wróbel, K., and Ignatiuk, D.: Glacier internal structure revealed by automatic image processing-powered classification of radar images, Applied Geomatics, 17, 677–692, https://doi.org/10.1007/s12518-025-00635-5, 2025.

Kamangir, H., Rahnemoonfar, M., Dobbs, D., Paden, J., and Fox, G.: Deep hybrid wavelet network for ice boundary detection in radra imagery, International Geoscience and Remote Sensing Symposium (IGARSS), 2018-July, 3449–3452, https://doi.org/10.1109/IGARSS.2018.8518617, iSBN: 9781538671504, 2018.

Karušs, J., Lamsters, K., Sobota, I., Ješkins, J., Džeriņš, P., and Hodson, A.: Drainage system and thermal structure of a High Arctic polythermal glacier: Waldemarbreen, western Svalbard, Journal of Glaciology, 68, 591–604, https://doi.org/10.1017/jog.2021.125, 2022.

Kingma, D. P. and Ba, J.: Adam: A Method for Stochastic Optimization, https://doi.org/10.48550/arXiv.1412.6980, arXiv:1412.6980 [cs], 2017.

Krizhevsky, A., Sutskever, I., and Hinton, G. E.: ImageNet Classification with Deep Convolutional Neural Networks, in: Advances in Neural Information Processing Systems, vol. 25, Curran Associates, Inc., https://proceedings.neurips.cc/paper/2012/hash/c399862d3b9d6b76c8436e924a68c45b-Abstract.html, 2012.

Kunz, K. S. and Luebbers, R. J.: The finite difference time domain method for electromagnetics, CRC press, 1993.

https://doi.org/10.5194/egusphere-2026-4083
Preprint. Discussion started: 21 July 2026

Lavrentiev, I. I., Glazovsky, A. F., Macheret, Y. Y., Matskovsky, V. V., and Muravyev, A. Y.: Reserve of ice in glaciers on the Nordenskiöld Land, Spitsbergen, and their changes over the last decades, Ice and Snow, 59, 23–38, https://doi.org/10.15356/2076-6734-2019-1-23-38, number: 1, 2019.

Lecun, Y., Bottou, L., Bengio, Y., and Haffner, P.: Gradient-based learning applied to document recognition, Proceedings of the IEEE, 86, 2278–2324, https://doi.org/10.1109/5.726791, 1998.

Lecun, Y., Bengio, Y., and Hinton, G.: Deep learning, Nature, 521, 436–444, https://doi.org/10.1038/nature14539, 2015.

Letamendia, U. and Ramírez, I.: Implementation of Automatic classification of the hydrothermal structure of polythermal glaciers from ground-penetrating radar using deep learning techniques, https://doi.org/10.5281/zenodo.21260762, 2026.

Letamendia, U., Navarro, F., and Benjumea, B.: Ground-penetrating radar as a tool for determining the interface between temperate and cold ice, and snow depth: a case study for Hurd-Johnsons glaciers, Livingston Island, Antarctica, Annals of Glaciology, pp. 1–9, https://doi.org/10.1017/aog.2023.73, 2023.

Letamendia, U., Ramírez Díaz, I., Navarro, F. J., Benjumea, B., Lavrentiev, I., and Schiavi, E.: Automatic classification of the hydrothermal structure of polythermal glaciers from ground-penetrating radar using deep learning techniques - Dataset, https://doi.org/10.5281/zenodo.21134524, 2026.

Lin, T.-Y., Dollár, P., Girshick, R., He, K., Hariharan, B., and Belongie, S.: Feature Pyramid Networks for Object Detection, https://doi.org/10.48550/arXiv.1612.03144, arXiv:1612.03144 [cs], 2017.

Long, J., Shelhamer, E., and Darrell, T.: Fully Convolutional Networks for Semantic Segmentation, https://doi.org/10.48550/arXiv.1411.4038, arXiv:1411.4038 [cs], 2015.

MacGregor, J. A., Boisvert, L. N., Medley, B., Petty, A. A., Harbeck, J. P., Bell, R. E., Blair, J. B., Blanchard-Wrigglesworth, E., Buckley, E. M., Christoffersen, M. S., Cochran, J. R., Csathó, B. M., De Marco, E. L., Dominguez, R. T., Fahnestock, M. A., Farrell, S. L., Gogineni, S. P., Greenbaum, J. S., Hansen, C. M., Hofton, M. A., Holt, J. W., Jezek, K. C., Koenig, L. S., Kurtz, N. T., Kwok, R., Larsen, C. F., Leuschen, C. J., Locke, C. D., Manizade, S. S., Martin, S., Neumann, T. A., Nowicki, S. M., Paden, J. D., Richter-Menge, J. A., Rignot, E. J., Rodríguez-Morales, F., Siegfried, M. R., Smith, B. E., Sonntag, J. G., Studinger, M., Tinto, K. J., Truffer, M., Wagner, T. P., Woods, J. E., Young, D. A., and Yungel, J. K.: The Scientific Legacy of NASA's Operation IceBridge, Reviews of Geophysics, 59, e2020RG000 712, https://doi.org/10.1029/2020RG000712, _eprint: https://agupubs.onlinelibrary.wiley.com/doi/pdf/10.1029/2020RG000712, 2021.

Macheret, Y., Glazovsky, A., and Lavrentiev, I.: Distribution of cold and temperate ice and water in glaciers at Nordenskiöld Land, Svalbard, according to data on ground-based radio-echo sounding, Bulletin of Geography. Physical Geography Series, pp. 77–90, https://doi.org/10.2478/bgeo-2019-0016, number: 17, 2019.

Martín-Espanol, A., Vasilenko, E. V., Navarro, F. J., Otero, J., Lapazaran, J. J., Lavrentiev, I., Macheret, Y. Y., and Machío, F.: Radio-echo sounding and ice volume estimates of western Nordenskiöld Land glaciers, Svalbard, Annals of Glaciology, 54, 211–217, https://doi.org/10.3189/2013AoG64A109, 2013.

Moholdt, G., Wesselink, D., and Aas, H. F.: Merged Svalbard digital terrain model, https://doi.org/10.21334/NPOLAR.2019.675565F7, 2019.

Moqadam, H., Steinhage, D., Wilhelm, A., and Eisen, O.: Going Deeper With Deep Learning: Automatically Tracing Internal Reflection Horizons in Ice Sheets—Methodology and Benchmark Data Set, Journal of Geophysical Research: Machine Learning and Computation, 2, e2024JH000 493, https://doi.org/10.1029/2024JH000493, 2025.

Murray, T., Stuart, G. W., Fry, M., Gamble, N. H., and Crabtree, M. D.: Englacial water distribution in a temperate glacier from surface and borehole radar velocity analysis, Journal of Glaciology, 46, 389–398, https://doi.org/10.3189/172756500781833188, 2000.

Navarro, F. and Eisen, O.: Ground-penetrating radar in glaciological applications, pp. 195–229, ISBN 978-0-415-40166-1, https://doi.org/10.1201/b10155-12, 2009.

Navarro, F., Martín-Español, A., Lapazaran, J., Grabiec, M., Otero, J., Vasilenko, E., and Puczko, D.: Ice volume estimates from ground-penetrating radar surveys, Wedel Jarlsberg Land glaciers, Svalbard, Arctic, Antarctic, and Alpine Research, 46, 394–406, https://doi.org/10.1657/1938-4246-46.2.394, 2014.

Navarro, F., Möller, R., Vasilenko, E., Martín-Español, A., Finkelnburg, R., and Möller, M.: Ice thickness distribution and hydrothermal structure of Elfenbeinbreen and Sveigbreen, eastern Spitsbergen, Svalbard, Journal of Glaciology, 61, 1015–1018, https://doi.org/10.3189/2015JoG15J141, 2015.

Navarro, F. J., Macheret, Y. Y., and Benjumea, B.: Application of radar and seismic methods for the investigation of temperate glaciers, Journal of Applied Geophysics, 57, 193–211, https://doi.org/10.1016/j.jappgeo.2004.11.002, 2005.

Ogier, C., Manen, D.-J. v., Maurer, H., Räss, L., Hertrich, M., Bauder, A., and Farinotti, D.: Ground penetrating radar in temperate ice: englacial water inclusions as limiting factor for data interpretation, Journal of Glaciology, pp. 1–12, https://doi.org/10.1017/jog.2023.68, 2023.

Pettersson, R., Jansson, P., and Holmlund, P.: Cold surface layer thinning on Storglaciären, Sweden, observed by repeated ground penetrating radar surveys, Journal of Geophysical Research: Earth Surface, 108, n/a–n/a, https://doi.org/10.1029/2003jf000024, 2003.

Pettersson, R., Jansson, P., and Blatter, H.: Spatial variability in water content at the cold-temperate transition surface of the polythermal Storglaciären, Sweden, Journal of Geophysical Research: Earth Surface, 109, n/a–n/a, https://doi.org/10.1029/2003JF000110, 2004.

Plewes, L. A. and Hubbard, B.: A review of the use of radio-echo sounding in glaciology, Progress in Physical Geography: Earth and Environment, 25, 203–236, https://doi.org/10.1177/030913330102500203, 2001.

Rahnemoonfar, M., Johnson, J., and Paden, J.: AI Radar Sensor: Creating Radar Depth Sounder Images Based on Generative Adversarial Network, Sensors, 19, 5479, https://doi.org/10.3390/s19245479, number: 24, 2019.

Rahnemoonfar, M., Yari, M., Paden, J., Koenig, L., and Ibikunle, O.: Deep multi-scale learning for automatic tracking of internal layers of ice in radar data, Journal of Glaciology, 67, 39–48, https://doi.org/10.1017/jog.2020.80, 2020.

RGI Consortium: Randolph Glacier Inventory - A Dataset of Global Glacier Outlines, Version 7, https://doi.org/10.5067/F6JMOVY5NAVZ, 2023.

Rumelhart, D. E., Hinton, G. E., and Williams, R. J.: Learning representations by back-propagating errors, Nature, 323, 533–536, https://doi.org/10.1038/323533a0, 1986.

Sandmeier: Reflexw - GPR and seismic processing software - Sandmeier, https://www.sandmeier-geo.de/reflexw.html, 2024.

Santin, I., Roncoroni, G., Forte, E., Gutgesell, P., and Pipan, M.: GPR modelling and inversion to quantify the debris content within ice, Near Surface Geophysics, n/a, https://doi.org/10.1002/nsg.12274, _eprint: https://onlinelibrary.wiley.com/doi/pdf/10.1002/nsg.12274, 2023.

Schannwell, C., Murray, T., Kulessa, B., Gusmeroli, A., Saintenoy, A., and Jansson, P.: An automatic approach to delineate the cold-temperate transition surface with ground-penetrating radar on polythermal glaciers, Annals of Glaciology, 55, 89–96, https://doi.org/10.3189/2014AoG67A102, 2014.

Sold, L., Huss, M., Hoelzle, M., Andereggen, H., Joerg, P. C., and Zemp, M.: Methodological approaches to infer end-of-winter snow distribution on alpine glaciers, Journal of Glaciology, 59, 1047–1059, https://doi.org/10.3189/2013JoG13J015, 2013.

Varshney, D., Rahnemoonfar, M., Yari, M., Paden, J., Ibikunle, O., and Li, J.: Deep learning on airborne radar echograms for tracing snow accumulation layers of the greenland ice sheet, Remote Sensing, 13, 1–21, https://doi.org/10.3390/rs13142707, 2021.

Vasilenko, E. V., Machío, F., Lapazaran, J. J., Navarro, F. J., and Frolovskiy, K.: A compact lightweight multipurpose ground-penetrating radar for glaciological applications, Journal of Glaciology, 57, 1113–1118, https://doi.org/10.3189/002214311798843430, 2011.

Vaswani, A., Shazeer, N., Parmar, N., Uszkoreit, J., Jones, L., Gomez, A. N., Kaiser, u., and Polosukhin, I.: Attention is All you Need, in: Advances in Neural Information Processing Systems, vol. 30, Curran Associates, Inc., https://proceedings.neurips.cc/paper/2017/hash/3f5ee243547dee91fbd053c1c4a845aa-Abstract.html, 2017.

Wang, Y., Xu, M., Paden, J. D., Koenig, L. S., Fox, G. C., and Crandall, D. J.: Deep Tiered Image Segmentation for Detecting Internal ICE Layers in Radar Imagery, in: 2021 IEEE International Conference on Multimedia and Expo (ICME), pp. 1–6, ISSN 1945-788X, https://doi.org/10.1109/ICME51207.2021.9428365, 2021.

Warren, C., Giannopoulos, A., and Giannakis, I.: gprMax: Open source software to simulate electromagnetic wave propagation for Ground Penetrating Radar, Computer Physics Communications, 209, 163–170, https://doi.org/10.1016/j.cpc.2016.08.020, 2016.

Warren, C., Giannopoulos, A., Gray, A., Giannakis, I., Patterson, A., Wetter, L., and Hamrah, A.: A CUDA-based GPU engine for gprMax: Open source FDTD electromagnetic simulation software, Computer Physics Communications, 237, 208–218, https://doi.org/10.1016/j.cpc.2018.11.007, 2019.

Watts, R. D. and England, A. W.: Radio-echo Sounding of Temperate Glaciers: Ice Properties and Sounder Design Criteria, Journal of Glaciology, 17, 39–48, https://doi.org/10.3189/s0022143000030707, 1976.

Xu, M., Fan, C., Paden, J. D., Fox, G. C., and Crandall, D. J.: Multi-task Spatiotemporal Neural Networks for Structured Surface Reconstruction, Proceedings - 2018 IEEE Winter Conference on Applications of Computer Vision, WACV 2018, 2018-Janua, 1273–1282, https://doi.org/10.1109/WACV.2018.00144, iSBN: 9781538648865, 2018.

Yari, M., Ibikunle, O., Varshney, D., Chowdhury, T., Sarkar, A., Paden, J., Li, J., and Rahnemoonfar, M.: Airborne Snow Radar Data Simulation With Deep Learning and Physics-Driven Methods, IEEE Journal of Selected Topics in Applied Earth Observations and Remote Sensing, 14, 12 035–12 047, https://doi.org/10.1109/JSTARS.2021.3126547, 2021.

Zhu, A., Zhao, W., Wang, B., and Cui, X.: Automatically classifying and extracting ice layers and bedrock interfaces from ice-penetrating radar data, Journal of Applied Geophysics, 250, 106 237, https://doi.org/10.1016/j.jappgeo.2026.106237, 2026.